

Near-eye Dual-layer Light Field Display

ANONYMOUS AUTHOR(S)

Abstract...

CCS Concepts: • **Computer systems organization** → **Embedded systems**; *Redundancy*; Robotics; • **Networks** → Network reliability;

Additional Key Words and Phrases: ACM proceedings, L^AT_EX, text tagging

ACM Reference format:

Anonymous Author(s). 2010. Near-eye Dual-layer Light Field Display. *ACM Trans. Graph.* 9, 4, Article 39 (March 2010), 5 pages.
https://doi.org/0000001.0000001_2

1 INTRODUCTION

Introduction...

1.1 Contributions

This paper makes the following contributions:

Contribution 1. Description of contribution 1.

Contribution 2. Description of contribution 2.

2 SPECTRAL ANALYSIS

2.1 Light field representation

The radiance of a light ray in 3d space at the position (x, y, z) and direction (u, v) can be represented by the plenoptic function $P(x, y, z, u, v)$. Following [Chai et al. 2000], the coordinates (u, v) are taken as the intersection of the ray with a plane orthogonal to the z direction at unit distance relative to (x, y, z) as depicted in figure ??.

The canonical 4d light field $L(x, y, u, v) = P(x, y, 0, u, v)$ describes the radiance reaching the plane $z = 0$. The values in $L(x, y, u, v)$ can be propagated to another plane at $z = z_{local}$ and define a local light field $L_{local}(x, y, u, v)$. Note that $L_{local}(x, y, u, v)$ is different from $P(x, y, z_{local}, u, v)$ due to occlusions and is described only by the radiance along rays in empty space reaching the plane $z = 0$.

We refer to (x, y) as *spatial* coordinates and to (u, v) as *angular* coordinates. Throughout this work we address a 2d spatio-angular slice of the light field, $L(x, u)$. The extension to the full 4d light field is mostly straightforward and any difference will be indicated whenever necessary.

As shown in figure ??, a local light field relates to the canonical light field by $L_{local}(x, u) = L(x - uz_{local}, u)$ or, in matrix representation, by eq. 1.

$$L_{local} \begin{pmatrix} x \\ u \end{pmatrix} = L \begin{pmatrix} 1 & -z_{local} \\ 0 & 1 \end{pmatrix} \begin{pmatrix} x \\ u \end{pmatrix} \quad (1)$$

We denote the spatial and angular frequencies as ω_x and ω_u , respectively. The local light field spectrum $\hat{L}_{local}(\omega_x, \omega_u)$ can then be described from the canonical light field spectrum $\hat{L}(\omega_x, \omega_u)$ (eq. 2).

A note.

2010. 0730-0301/2010/3-ART39 \$15.00
https://doi.org/0000001.0000001_2

$$\hat{L}_{local} \begin{pmatrix} \omega_x \\ \omega_u \end{pmatrix} = \hat{L} \begin{pmatrix} 1 & 0 \\ z_{local} & 1 \end{pmatrix} \begin{pmatrix} \omega_x \\ \omega_u \end{pmatrix} \quad (2)$$

2.2 Perceived image spectrum

Images can be synthesized by selecting and combining rays from the light field. In this subsection we describe what an observer would see for a given light field reaching his pupil. Given the position and orientation of the observer, we choose to place the canonical light field over the pupil and orthogonal to the observer main optical axis (fig. ??).

We assume a thin lens camera model with the retina at z_r and the pupil lens giving focus at an arbitrary distance z_f . The light field reaching the retina can be described by the local light field on the plane at focus (eq. 3). Using eq. 1 and eq. 3, the retina light field can be described by the light field reaching the pupil (eq. 4).

$$L_r \begin{pmatrix} x \\ u \end{pmatrix} = L_f \begin{pmatrix} \frac{z_f}{z_r} & 0 \\ \frac{1}{z_r} - \frac{1}{z_f} & \frac{z_r}{z_f} \end{pmatrix} \begin{pmatrix} x \\ u \end{pmatrix} \quad (3)$$

$$L_r \begin{pmatrix} x \\ u \end{pmatrix} = L_p \begin{pmatrix} 1 & -z_r \\ \frac{1}{z_r} - \frac{1}{z_f} & \frac{z_r}{z_f} \end{pmatrix} \begin{pmatrix} x \\ u \end{pmatrix} \quad (4)$$

The pupil light field is equal to the canonical light field with the rays outside of the pupil aperture being blocked, viz., $L_p(x, u) = L(x, u) \text{rect}(\frac{x}{a})$. Where a is the pupil aperture diameter and $\text{rect}(x) = 1$ for $|x| < 0.5$ and 0 otherwise. Finally, the retina light field can be described by the canonical light field (eq. 5).

$$L_r \begin{pmatrix} x \\ u \end{pmatrix} = L \begin{pmatrix} 1 & -z_r \\ \frac{1}{z_r} - \frac{1}{z_f} & \frac{z_r}{z_f} \end{pmatrix} \begin{pmatrix} x \\ u \end{pmatrix} \text{rect} \left(\frac{x - uz_r}{a} \right) \quad (5)$$

The image formed on the retina is given by the integration of the retina light field over the angular coordinate (eq. 6). Applying eq. 6 inside the definition of the image spectrum we have eq. 7.

$$I(x) = \int_{-\infty}^{\infty} L_r(x, u) du \quad (6)$$

$$\begin{aligned} \hat{I}(\omega_x) &= \int_{-\infty}^{\infty} I(x) e^{-2\pi i \omega_x x} dx = \\ &= \iint_{-\infty}^{\infty} L_r(x, u) e^{-2\pi i \omega_x x} dx du \end{aligned} \quad (7)$$

Given that the retina light field spectrum can be written, by definition, as in eq. 8. Comparing eq. 7 and eq. 8, we can assert that $\hat{I}(\omega_x) = \hat{L}_r(\omega_x, 0)$.

$$\hat{L}_r(\omega_x, \omega_u) = \iint_{-\infty}^{\infty} L_r(x, u) e^{-2\pi i \omega_x x} e^{-2\pi i \omega_u u} dx du \quad (8)$$

From eq. 4, the retina light field spectrum can be written as in eq. 9 and thus the image spectrum can be written as in eq. 10, where δ

denotes the Dirac delta function and $*$ denotes the two dimensional convolution operation over (ω_x, ω_u) .

$$\hat{L}_r \begin{pmatrix} \omega_x \\ \omega_u \end{pmatrix} = \hat{L}_p \begin{pmatrix} \frac{z_r}{z_f} & \frac{1}{z_f} - \frac{1}{z_r} \\ z_r & 1 \end{pmatrix} \begin{pmatrix} \omega_x \\ \omega_u \end{pmatrix} \quad (9)$$

$$\begin{aligned} \hat{I}(\omega_x) &= \hat{L}_r \begin{pmatrix} \omega_x \\ 0 \end{pmatrix} = \hat{L}_p \begin{pmatrix} \frac{z_r}{z_f} \omega_x \\ z_r \omega_x \end{pmatrix} = \\ &= \hat{L} \begin{pmatrix} \frac{z_r}{z_f} \omega_x \\ z_r \omega_x \end{pmatrix} * \left[a \operatorname{sinc} \left(a \frac{z_r}{z_f} \omega_x \right) \delta(z_r \omega_x) \right] \end{aligned} \quad (10)$$

The final discrete image is a sampling of the continuous image signal formed on the retina. The maximum frequency ξ_x which can be represented without aliasing is determined from the image sampling rate through Nyquist-Shannon theorem.

Regardless of the focus distance z_f , the maximum angular frequency on the canonical light field which can still be represented in the image without aliasing is $z_r \xi_x$. Therefore, when sampling the canonical light field for an observer (with unknown and possibly dynamic focus distance), one should not be concerned about capturing angular frequencies above $z_r \xi_x$.

Taking the full 4d light field into account, if the 2d retina image is sampled in a rectangular lattice (like a camera), then the non-vanishing intervals of horizontal and vertical spatial frequencies (ω_x, ω_y) are separable and the 4d light field spectrum is the product of two separate spectra of 2d spatio-angular slices as described above. The maximum angular frequencies to be captured in the 4d canonical light field are $\omega_u = z_r \xi_x$ and $\omega_v = z_r \xi_y$.

On the other hand, if the 2d image is sampled in a hexagonal lattice (like the human eye), the image spectral support is not separable and neither is the spectral support for the 4d canonical light field. Even so, the 4d canonical light field angular components are still bandlimited and independent of focus distance. In any case, an artificial rectangular spectral support containing the actual image spectrum can be assumed, allowing the light field spectrum to be separable into two spatio-angular slices at the cost of higher sampling rates.

2.3 Bounded Lambertian scene

3 LIGHT FIELD REPRESENTATION

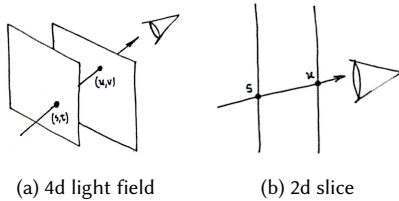


Fig. 1. Two-plane parameterization

Following the notation in [Gortler et al. 1996; Levoy and Hanrahan 1996] we use the global two-plane parameterization. A light ray $l(s, t, u, v)$ is then defined by its intersections with two parallel planes (figure 1a). We will refer to the coordinates on the plane

closer to the observer as the *angular* coordinates (u, v) and on the farther as the *spatial* coordinates (s, t) .

Throughout this work we address a 2d spatio-angular light field slice (figure 1b). The extension to the full 4d light field is mostly straightforward and any difference will be indicated whenever necessary. Also, with no loss of generality, we assume the planes to be one unit apart.

3.1 Local parameterization

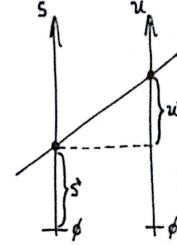


Fig. 2. Relationship between global parameters (s, u) and local parameters (s', u')

Some related works use a local two-plane parameterization [Chai et al. 2000]. On those cases the spatial coordinates are absolute while the angular coordinates are taken relative to the spatial coordinates (figure 2). This induces a shear on the angular coordinates when compared to the global parameterization, $l(s, t) = l(s', s' + u')$. Accordingly, on the frequency domain there will be a shear on the spatial components, $\hat{I}(\omega_s, \omega_u) = \hat{I}(\omega_{s'} - \omega_{u'}, \omega_{u'})$. Bearing this in mind, all conclusions remain the same with minor modifications. It is also important to notice that the terms spatial and angular (or directional) are sometimes swapped since their meanings are a matter of interpretation.

4 FOURIER SPECTRUM ANALYSIS

Many previous works analysed the light field spectrum for scenes with different levels of complexity [Chai et al. 2000; Durand et al. 2005; Liang and Ramamoorthi 2015; Ng 2005]. In this section, we review the spectrum for a single Lambertian surface as well as for Lambertian scenes free of occlusions.

4.1 Lambertian surface

Considering a surface parallel to the light field parameterization planes and at a distance d from the angular plane (figure 3a), a ray intersects this surface on $x = ds + (1-d)u$. If the surface is Lambertian and $f(x)$ denotes the radiance of any ray passing through x , then $l(s, u) = f(ds + (1-d)u)$. Thus, the Fourier transform of the light field will be $\hat{I}(\omega_s, \omega_u) = \hat{f}(\omega_s/d) \delta((1 - \frac{1}{d})\omega_s + \omega_u)$. From this we can draw two important conclusions: The spectrum of the Lambertian surface lies in the line $\omega_u = (\frac{1}{d} - 1)\omega_s$ and $\omega_s = d\omega_x$.

Restricting the frequency ω_x on the surface makes the light field bandlimited. If the maximum frequency on the surface is ξ_x then the light field spectrum becomes a line segment as shown in figure 3b.

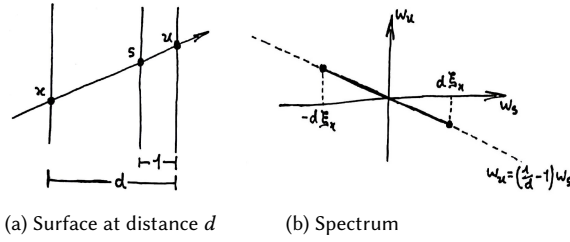


Fig. 3. Single lambertian surface

4.2 Bounded scene

A Lambertian scene between a maximum distance d_{max} and minimum distance d_{min} can be decomposed as infinite Lambertian surfaces stacked. Without taking visibility into account, the light field spectrum is bounded by the lines $\omega_u = (\frac{1}{d_{max}} - 1)\omega_s$ and $\omega_u = (\frac{1}{d_{min}} - 1)\omega_s$ (figure 4). Even though occlusions can introduce high frequencies [Durand et al. 2005], this effect will be ignored as in [Chai et al. 2000].

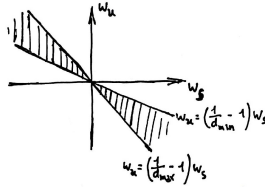


Fig. 4. Bounded scene spectrum

5 RENDERING

Images can be synthesized by selecting and combining rays from the light field. Assuming the position of the observer is known, we place the angular plane and the spatial plane at the distances 0 and 1 from it, respectively. Both planes are orthogonal to the observer main optical axis. Parallel to the parameterization planes will be the observer image plane, at a distance d_i on the opposite direction (figure 5).

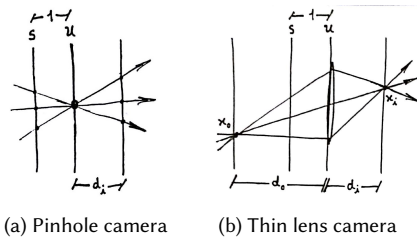


Fig. 5. Camera models

5.1 Pinhole camera

For a pinhole camera model, the rays intersecting the observer image plane are the rays with $u = 0$ (figure 5a). The point with coordinate

x_i on the image plane receives a single ray described as $l(x_i/d_i, 0)$. Therefore, the frequency ω_i on the image plane is related to the spatial frequency by $\omega_i = \omega_s/d_i$.

5.2 Thin lens camera

For a thin lens camera model, the lens will be giving focus to a plane at an arbitrary distance d_o (figure 5b). The coordinate x_i on the image plane will correspond to $x_o = \frac{d_o}{d_i}x_i$ on the plane at focus. All rays radiating from x_o will be integrated over the angular coordinate (where the lens is located) in order to determine the pixel value in the sensor. On the frequency domain this correspond to a slice of the light field spectrum closely related to the spectrum of a Lambertian plane as described in subsection 4.1 at a distance d_o . Likewise, $\omega_u = (\frac{1}{d_o} - 1)\omega_s$ and $\omega_s = d_o\omega_o$.

From the correspondence between x_o and x_i we have $\omega_o = \frac{d_i}{d_o}\omega_i$ and thereby $\omega_i = \omega_s/d_i$ (like the pinhole camera model). Even though the slope of the slice depends on the distance d_o , the frequency ω_i in the image does not.

In practice, the lens has a finite aperture that imposes bounds on the integration over the angular coordinate. Instead of dealing with those bonds directly in the integral, we can keep integrating over the entire angular plane by multiplying beforehand the light field by a *box* filter defined solely by the angular coordinate. This multiplication corresponds to a convolution with a *sinc* filter on the angular component of the frequency, keeping in this way the spatial frequency ω_s , and ergo the frequency on the image ω_i , still independent from the distance d_o .

5.3 Discrete image

The final discrete image is a sampling of the continuous image signal reaching the sensor. The image sampling rate determines by Nyquist-Shannon theorem the maximum frequency ξ_i which can be represented without aliasing.

Regardless of the camera model, $\omega_i = \omega_s/d_i$ implies that a spatial frequency above $\xi_s = d_i\xi_i$ results in aliasing. Therefore, we assume that the light field does not contain spatial frequencies above ξ_s or that it was prefiltered accordingly.

This restriction combined with the bounded Lambertian scene restrictions from subsection 4.2 turns the light field spectrum bandlimited (figure 6).

Regarding the 4d light field, if the 2d image is sampled in a rectangular lattice (like a camera), then the horizontal and vertical spatial frequency bounds are seperable and the 4d light field spectrum is the product of two separate 2d light field spectrum as described. On the other hand, if the 2d image is sampled in a hexagonal lattice (like the human eye), the spatial frequency bounds are not seperable and neither is the 4d light field spectrum. Even so, the light field spectrum is still bandlimited.

6 SAMPLING AND FILTERING

From the light field spectral analysis, different light field sampling strategies can be employed. In this section we review three strategies and their corresponding reconstruction kernels.

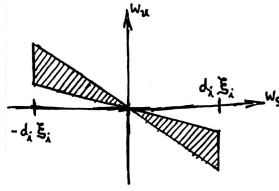


Fig. 6. Bandlimited light field

6.1 Naive box filter

The most straightforward approach is to sample the scene in a rectangular lattice over the angular and spatial coordinates. In order to prevent aliasing, the sampling rates needs to be so that the light field spectrum can be reconstructed by a box filter as in figure 7.

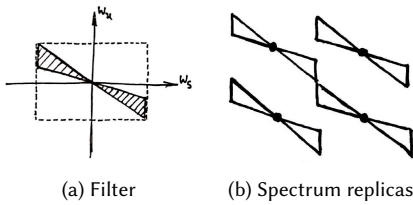


Fig. 7. Naive box filter

6.2 Optimum box filter

As proposed by [Chai et al. 2000], the sampling rates can be reduced by changing the plane over which the sampling is done instead of the spatial plane. The optimal sampling rate is achieved for a plane at a distance $d_m = \frac{2}{\frac{1}{d_{min}} + \frac{1}{d_{max}}}$. The box filter over the angular frequency ω_u and the frequency on the sampling plane ω_m (figure 9a) is sheared over the coordinates ω_u and ω_s (figure 8a) giving a more compact selection of the spectrum and allowing the spectrum replicas to be closer together (figures 8b and 9b).

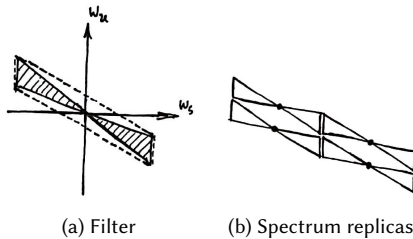


Fig. 8. Optimum box filter (light field coordinates)

6.3 Optimum arbitrary shape filter

The spectrum replicas can be arranged even closer together, covering all the frequency domain without any gaps (figures 10b and 11b). In this arrangement the signal can not be reconstructed with a box filter. A custom filter needs to be designed to match the exact shape of the spectrum (figures 10a and 11a) as proposed by [Zhang and Chen

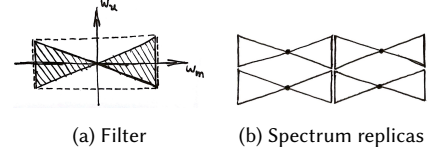


Fig. 9. Optimum box filter (sampling coordinates)

2001]. Nonetheless, the sampling is still rectangular (figure 11b) for the right coordinates, in this case over the planes at distances d_{min} and d_{max} .

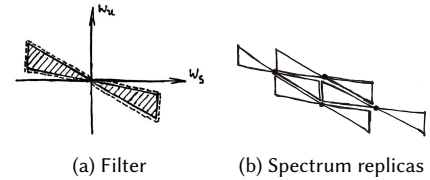


Fig. 10. Optimum arbitrary shape filter (light field coordinates)

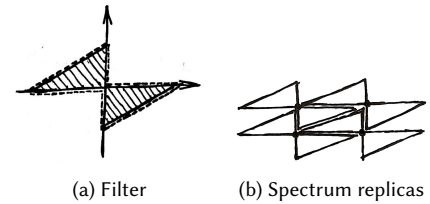


Fig. 11. Optimum arbitrary shape filter (sampling coordinates)

7 DUAL-LAYER AUTOMULTISCOPIC DISPLAY

[Lanman et al. 2010]

A new family of compressive light field displays called tensor displays was introduced by [Wetzstein et al. 2012]. Multiple layers of LCD panels are stacked, each attenuating the rays emitted by a backlight. The

7.1 Multiplicative modulation

7.2 Non-negative factorization

7.3 Time-multiplexing

7.4 The light field stereoscope

7.5 Ray interpolation/integration

8 EXPERIMENTS

9 CONCLUSION AND FUTURE WORK

Conclusion...

REFERENCES

Jin-Xiang Chai, Xin Tong, Shing-Chow Chan, and Heung-Yeung Shum. 2000. Plenoptic Sampling. In *Proceedings of the 27th Annual Conference on Computer Graphics and Interactive Techniques (SIGGRAPH '00)*. ACM Press/Addison-Wesley Publishing Co., New York, NY, USA, 307–318. <https://doi.org/10.1145/344779.344932>

- Frédo Durand, Nicolas Holzschuch, Cyril Soler, Eric Chan, and François X. Sillion. 2005. A Frequency Analysis of Light Transport. *ACM Trans. Graph.* 24, 3 (July 2005), 1115–1126. <https://doi.org/10.1145/1073204.1073320>
- Steven J. Gortler, Radek Grzeszczuk, Richard Szeliski, and Michael F. Cohen. 1996. The Lumigraph. In *Proceedings of the 23rd Annual Conference on Computer Graphics and Interactive Techniques (SIGGRAPH '96)*. ACM, New York, NY, USA, 43–54. <https://doi.org/10.1145/237170.237200>
- Douglas Lanman, Matthew Hirsch, Yunhee Kim, and Ramesh Raskar. 2010. Content-adaptive Parallax Barriers: Optimizing Dual-layer 3D Displays Using Low-rank Light Field Factorization. *ACM Trans. Graph.* 29, 6, Article 163 (Dec. 2010), 10 pages. <https://doi.org/10.1145/1882261.1866164>
- Marc Levoy and Pat Hanrahan. 1996. Light Field Rendering. In *Proceedings of the 23rd Annual Conference on Computer Graphics and Interactive Techniques (SIGGRAPH '96)*. ACM, New York, NY, USA, 31–42. <https://doi.org/10.1145/237170.237199>
- Chia-Kai Liang and Ravi Ramamoorthi. 2015. A Light Transport Framework for Lenslet Light Field Cameras. *ACM Trans. Graph.* 34, 2, Article 16 (March 2015), 19 pages. <https://doi.org/10.1145/2665075>
- Ren Ng. 2005. Fourier Slice Photography. *ACM Trans. Graph.* 24, 3 (July 2005), 735–744. <https://doi.org/10.1145/1073204.1073256>
- Gordon Wetzstein, Douglas Lanman, Matthew Hirsch, and Ramesh Raskar. 2012. Tensor Displays: Compressive Light Field Synthesis Using Multilayer Displays with Directional Backlighting. *ACM Trans. Graph.* 31, 4, Article 80 (July 2012), 11 pages. <https://doi.org/10.1145/2185520.2185576>
- Cha Zhang and Tsuhan Chen. 2001. *Generalized Plenoptic Sampling*. Technical Report. Carnegie Mellon University, Pittsburgh, PA, USA.